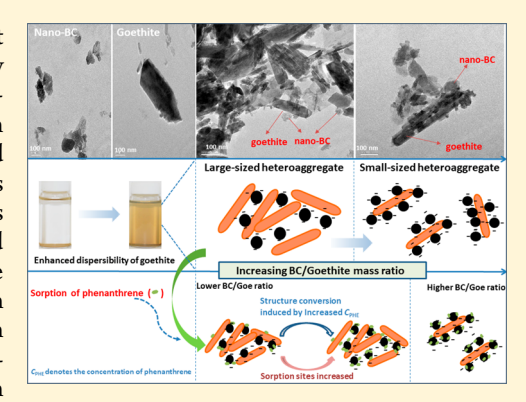


# New Insights into Black Carbon Nanoparticle-Induced Dispersibility of Goethite Colloids and Configuration-Dependent Sorption for **Phenanthrene**

Fei Lian, †,‡ Wenchao Yu, Shenyu Wang,† and Baoshan Xing\*,‡

Supporting Information

ABSTRACT: Black carbon nanoparticles (nano-BC) are one of the most active components in pyrogenic carbonaceous matter and involved in many biogeochemical processes. This study investigated heteroaggregation of nano-BC with goethite (a model of natural mineral colloids) and the configuration effect of heteroaggregates on phenanthrene (PHE) sorption. Nano-BC could significantly enhance the dispersion of goethite via heteroaggregation when its concentration was higher than the critical concentration  $(C_c)$ . The  $C_c$  was dependent on the surface potential of nano-BC, which was directly measured for the first time in this study. Configuration and stability of the heteroaggregates were regulated by BC-goethite mass ratio and solution pH. At pH 5.3, oppositely charged goethite and nano-BC interacted with each other through electrostatic attraction and the configuration of heteroaggregates was dependent on BC-goethite mass ratio. At pH 7.4, where both goethite and nano-BC were negatively charged, they heteroaggregated with



each other mainly through H-bonding and Lewis acid-base mechanisms, and the configuration of heteroaggregates was independent of BC-goethite mass ratio. For PHE sorption, small-sized heteroaggregates were more favorable than large ones due to the higher content of active sorption sites. Interestingly, at a higher concentration of PHE, we found that the solute molecules could probably penetrate into and/or alter the configuration of heteroaggregates and enhance its sorption capacity for PHE. These findings are useful for understanding the effect of nano-BC on colloidal stability and organic compound sorption of minerals.

#### INTRODUCTION

Black carbon (BC), the carbonaceous solid of biomass residue from incomplete combustion, is ubiquitous in the environment. Especially biochar, the man-made BC, is produced much more than ever before for various environmental and agricultural purposes including adsorption of contaminants,<sup>1</sup> carbon sequestration,<sup>2</sup> and soil modifiers.<sup>3</sup> Statistically, the global production of BC is estimated to be 50-270 Tg per year, and the majority of the products would remain in the soil environment.<sup>4</sup> Although BC is recalcitrant to mineralization, a fraction of this charred material can be discharged and mobilized in aquatic environments as dissolved BC (DBC), 5-7 which amounts to ca. 10% of the dissolved organic carbon in rivers and >2% in oceans.<sup>8,9</sup> Furthermore, bulk BC can even be physically disintegrated into BC nanoparticles (nano-BC) with size smaller than 100 nm driven by aging and weathering in the environment.<sup>10</sup> Considering the high mobility and reactivity of both DBC and nano-BC, 11 it is expected that they would greatly affect many biogeochemical processes in environments

such as contaminant transport, 12 element cycling, 13 and stability of natural colloids.14

It has been suggested that these ultrafine BC fractions have relatively high stability in aquatic environments. 15,16 For example, critical coagulation concentration (CCC) of nano-BC derived from pecan shells was 250 and 8.5 mmol/L for Na<sup>+</sup> and Ca<sup>2+</sup>, respectively, <sup>17</sup> higher than those of engineered carbon nanomaterials including carbon nanotube, 18 fullerene  $(C_{60})_{1}^{19}$  and graphene oxide  $(GO)_{1}^{20}$  Xu et al. 15 reported that no significant aggregation of DBC was observed when the concentration of NaCl was up to 800 mmol/L. On the other hand, naturally occurring colloids are present in almost all surface waters, the transport and fate of which is vital for understanding the key environmental processes in water/soil systems.<sup>14</sup> Nano-BC is negatively charged and likely out-

September 9, 2018 Received: Revised: December 1, 2018 Accepted: December 12, 2018 Published: December 12, 2018

<sup>&</sup>lt;sup>†</sup>Institute of Environmental Processes and Pollution Control and School of Environmental and Civil Engineering, Jiangnan University, Wuxi 214122, P. R. China

<sup>\*</sup>Stockbridge School of Agriculture, University of Massachusetts, Amherst, Massachusetts 01003, United States

<sup>&</sup>lt;sup>§</sup>College of Environmental Science and Engineering, Nankai University, Tianjin 300071, P. R. China

numbered by natural colloids (e.g., minerals) in real environmental media, and it is foreseeable that heteroaggregation with oppositely charged colloids (e.g., iron oxides) would be more likely to occur and have more profound environmental implications relative to homoaggregation of nano-BC. Heteroaggregation of other carbon nanoparticles (such as GO, carbon dots, and carbon nanotubes) with mineral colloids in aqueous solutions has been investigated. 21-24 It is found that carbon nanoparticles are likely to aggregate with minerals via different interactions including electrostatic attraction, <sup>21</sup> hydrogen bonding, and Lewis acid-base forces.<sup>22</sup> Heteroaggregation with minerals generally decreases the colloidal stability of these carbon materials and leads to their sedimentation because of the reduced electrostatic repulsion. Conversely, an interesting question confronting us is if the attached carbon nanoparticles could in turn contribute to the suspension of minerals in aqueous solutions. Feng et al.<sup>23</sup> reported that negatively charged GO could attach to the surface of positively charged hematite to form "electrostatic patches", which could partially neutralize its surface positive charges. Theoretically, if sufficient negatively charged nano-BC attaches to the mineral, its surface charge can be reversed, 17 which can increase the dispersibility of minerals. In that case, it is crucial to determine the critical concentration of nano-BC above which the minerals can be effectively dispersed by attached nano-BC. This information has profound significance for exploring the role of nano-BC in the transport and fate of natural colloids in the real environment. Although numerous studies have assessed the influence of dissolved organic matter (DOM) on the transport and stability of various colloids (listed in Table S1) in soils, it would be inaccurate to extrapolate these results to the interactions between nano-BC and minerals. Nano-BC is derived from pyrogenic carbon, whose property is distinct from that of natural DOM.<sup>25</sup> Strictly, it is also different from DBC (size <0.45  $\mu$ m), <sup>26</sup> which contains both "undissolved" particulates (i.e., nano-BC) and water-soluble fractions. We mainly focus on the aggregation between solid particles in the present study; hence, a combined procedure of sedimentation and centrifugation is selected to separate nano-BC from the residue of BC. We hypothesize that nano-BC could serve as a "natural dispersing agent" to greatly enhance the dispersibility of natural colloids through coassembling in aqueous environments.

Additionally, it is still unclear how and to what extent the attached nano-BC would affect the sorption behavior of mineral colloids. It is well-known that BC has higher sorption affinity for hydrophobic organic compounds (HOCs) than minerals. 27-29 However, it is worth noting that incorporation of nano-BC may not simply increase the sorption capacity of minerals because the configuration of newly formed BCmineral heteroaggregates would also affect the sorption of HOCs. It is suggested that ordered assembly can be formed between carbonaceous nanomaterials and mineral colloids in environmental media. 17,30,31 For example, binary wires and closed-packed structures were produced due to the association of C<sub>60</sub> to pure and humid acid coated iron oxide colloids.<sup>30</sup> Yi et al. 17 observed that nano-BC could heteroaggregate with CeO<sub>2</sub> nanoparticles through a charge neutralization-charge reversal mechanism at pH 5.3, while a charge-accumulation, core-shell structure was formed at pH 7.1. Thus, the configuration effect of BC-mineral mixtures on organic compound sorption merits further investigation.

Therefore, the overarching goals of the current work were to (1) examine the colloidal stability of nano-BC produced at different heat treatment temperatures (HTTs); (2) quantitatively investigate the heteroaggregation of nano-BC with a common mineral colloid (goethite); and (3) reveal the sorption mechanism(s) of BC-goethite heteroaggregates for HOCs. The nano-BC in this study was fractionated from rice straw biochar prepared under two different HTTs, which were systematically characterized by various techniques. Kinetics of nano-BC homoaggregation and its heteroaggregation with goethite were determined with and without the presence of mono- and divalent cations. Sorption of phenanthrene (PHE) on the BC-goethite mixtures was measured for better understanding the formation of the heteroaggregates and the related configuration effect on organic compound sorption.

# **■ EXPERIMENTAL SECTION**

Nano-BC Preparation. Rice straw, a typical agricultural biomass waste, was selected as the raw material for biochar production. Prior to use, the rice straw was washed with deionized (DI) water several times to remove surface impurities. After being oven-dried at 80 °C, the material was crushed and passed through a 2.0 mm mesh. Then the powdered straw was fed into a lab-scale tubular reactor within a muffle furnace and slowly pyrolyzed (10 °C/min) in a  $\rm N_2$  atmosphere at a desired temperature (400 or 700 °C) for 120 min. The obtained biochar was ground, sieved through a 150  $\mu$ m mesh, and referred to as bulk400 and bulk700, respectively.

The fractionation of nano-BC was conducted by a combined procedure of sedimentation and centrifugation. First, 50 g of the obtained biochar was added to 1 L of DI water and stirred (150 rpm) at room temperature for 24 h. After sonication (1 h at 120 W), the suspension was slowly poured through a 50  $\mu$ m sieve and the remaining particles were carefully washed with DI water to ensure that most of the desired fractions ( $<50 \mu m$ ) can pass through the sieve. After being oven-dried, the remaining particles were collected and used for other purposes. The filtered suspension was transferred into a glass beaker, added with DI water to 3 L, and then sonicated for another 1 h. The obtained suspension was left to sedimentation for 2 h to settle most of the bulk biochar particles based on Stoke's Law. The upper layer of suspension (0-10 cm from the surface) was siphoned off and then refilled with DI water to 3 L. This siphoning procedure was repeated 5-10 times until the upper layer of suspension became clear and had negligible Tyndall effect.<sup>32</sup> All the siphoned suspensions were combined and centrifuged at 10 000 rpm for 30 min. The supernatant was carefully collected and freeze-dried to obtain nano-BC. The centrifuge speed and duration were optimized according to Stoke's Law, and particle sizes of obtained nanoparticles were verified by a high-resolution transmission electron microscope (HRTEM) (JEOL, Japan) and dynamic light scattering (DLS) analyzer (90Plus, Brookhaven, U.S.A.). The obtained samples were referred to as nano400 and nano700, respectively. The stock suspension of nano-BC was prepared by stirring 50 mg of nano400 or nano700 in 500 mL of DI water overnight and then sonicating for 1 h. The total organic carbon (TOC) content of the suspensions was  $14.8 \pm 0.38$  and  $28.3 \pm 0.14$ mg TOC/L for nano400 and nano700, respectively, measured by a TOC analyzer (Shimadzu, Japan). The pH of both nano400 and nano700 suspensions was ~5.3.

**Mineral Colloid Preparation.** Goethite, purchased from Sigma-Aldrich, was used as a model clay mineral. To remove

organic matter from clay surface, 50 g of goethite was mixed with a solution containing 100 mL of DI water and 100 mL of  $H_2O_2$  (30 wt %) for 2 h in a 2 L beaker. Then the sample was rinsed thoroughly with DI water, vacuum-filtrated, freeze-dried, and passed through a 150  $\mu$ m sieve.

Homo- and Heteroaggregation Measurements. A time-resolved DLS technique was employed to examine the homoaggregation kinetics of nano-BC and its heteroaggregation rate with goethite using the DLS analyzer. The suspension of nano-BC and goethite was sonicated, respectively, in a bath sonicator with ice cooling before conducting the DLS measurements. The homoaggregation kinetics of nano-BC was measured by introducing 1 mL of the suspension with a concentration of 20 mg/L into disposable plastic cuvettes (Fisher, U.S.A.), and then 1 mL of NaCl or CaCl<sub>2</sub> solution with different concentrations was combined with the BC suspension in the cuvettes. After being briefly shaken, the cuvette was immediately inserted into the DLS cell to start the measurement. To investigate the influence of goethite on nano-BC stability, the above BC suspension was replaced by a BC-goethite mixture to conduct the DLS examination. The DLS measurements were sustained from 10 to 120 min at different time intervals and performed 6 times for each measurement. Attachment efficiencies  $(\alpha)$  were used to quantify the homoaggregation kinetics of nano-BC. The detailed determination of  $\alpha$  and CCC of nano-BC is presented in the Supporting Information.

Heteroaggregation of nano-BC and goethite was carried out by introducing nano-BC into goethite suspension and then immediately examined by the DLS analyzer. The final concentration of goethite was 50 mg/L, while that of nano400 and nano700 increased from 0.1 to 2.0 mg TOC/L and 0.16 to 3.2 mg TOC/L, respectively, which resulted in the mass ratios of BC to goethite in the range of 0.002-0.04 for nano400 and 0.0032-0.064 for nano700, respectively. Note that the TOC content of nano-BC was employed to calculate the mass ratio. During the heteroaggregation, the scattered light intensity of goethite suspension is significantly higher than that of nano-BC, probably due to the intrinsically lower ability of BC to scatter light relative to metallic particles and the larger size of goethite. Thus, the recorded hydrodynamic diameters  $(D_h)$  and zeta potential in the process of heteroaggregation mainly represent those of the goethite colloid, which can be demonstrated by the  $D_h$  measurement of goethite with and without nano400 or nano700 (Figure S1).

Attachment of Nano-BC on Goethite. The attachment of nano-BC on goethite was quantified to further elucidate the mechanism of their heteroaggregation. The attachment experiment was carried out in 20 mL screw cap vials at 25 °C and unadjusted pH condition according to previous studies.21,33 Briefly, 20 mg of goethite was added into the vials that already contained 15 mL of nano-BC suspensions with different concentrations (0-10 mg TOC/L). The solid/ liquid ratio was carefully selected in the preliminary experiment to achieve the removal of nano-BC between 20 and 80%. The vials were shaken at a speed of 200 rpm for 24 h to reach equilibrium (Figure S2) and then centrifuged at 3000 rpm for 20 min to separate the goethite and BC-goethite aggregates from the supernatants, while the free nano-BC remained stable in the supernatants. The BC concentrations in the supernatants were determined by a TOC analyzer. The mass of attached nano-BC was calculated by mass balance. All the experiments were performed in duplicate.

**Characterization.** Surface chemical composition of nano400 and nano700 was determined using X-ray photoelectron spectrometer (XPS) (PHI 5000 VersaProbe, Japan). Binding energies were calibrated by C 1s hydrocarbon peak at 284.8 eV. Deconvolution of C 1s spectra was conducted by XPSPEAK software. Brunauer-Emmett-Teller (BET) surface area  $(S_{BET})$  and total pore volume  $(V_{tot})$  were measured by nitrogen adsorption-desorption at 77 K using an Autosorb-1 gas analyzer (Quantachrome, U.S.A.). The functional groups were characterized using Fourier transform infrared spectroscopy (FTIR) (Nexus 870, Nicolet, U.S.A.) with 4 cm<sup>-1</sup> resolution in the range of 400 and 4000 cm<sup>-1</sup>. Raman spectra were obtained using a Renishaw Ramnascope (RM 2000, Wotton-under-Edge, U.K.). Surface morphologies of the nano-BC, goethite, and their heteroaggregates were observed by HRTEM with optimal resolution of 2 nm at 300 kV. D<sub>b</sub>, electrophoretic mobility (EPM), and zeta potential of the particles were determined in DI water by the DLS analyzer.

**Sedimentation Kinetics.** The dispersion and sedimentation of goethite in the suspension of nano-BC were measured by monitoring changes in optical absorbance as a function of time using UV-vis spectroscopy. The concentration of goethite remained constant (1000 mg/L), while that of nano400 and nano700 increased from 0 to 11.68 mg TOC/L and 15.69 mg TOC/L, respectively, at pH 5.3 and 7.4. The suspensions of BC and goethite were mixed using a shaking incubator at 150 rpm for 30 min. Then, 3 mL of the suspension was pipetted into a quartz cuvette and measured by a UV-vis spectrometer (Agilent 8453, U.S.A.) at 800 nm, where the nano-BC had little absorbance. The absorbance was recorded over 48 h at different time intervals to determine the effect of nano-BC on the sedimentation rates of goethite.

**Sorption of PHE.** A batch equilibrium technique was used to compare the sorption capacity of nano-BC with goethite for PHE. Details of the sorption procedure are presented in the Supporting Information. Single-point sorption was carried out to explore the configuration effect of BC-goethite heteroaggregates on PHE sorption. Briefly, an aliquot of goethite (2 mg) and 40 mL of nano-BC suspension with different concentrations, i.e., 0-2 mg TOC/L for nano400 and 0-3.2 mg TOC/L for nano700, respectively, were added into the 40 mL vials. After being shaken at 200 rpm for 1 h, the vials received a certain volume (<0.1%) of PHE stock solution (1.0 mg/L) in methanol. Different initial concentrations of PHE (0.263, 0.526, and 0.79 mg/L) were used to ensure the data compatibility and analytical accuracy. The vials were shaken in the dark at 25 °C for 7 days to achieve apparent sorption equilibrium. After centrifugation (15 000 rpm, 30 min) and filtration, the concentrations of PHE in the supernatant were determined by a Shimadzu Prominence liquid chromatography system with a diode array detector (reversed phase C18, 3.0 × 150 mm, 2.7  $\mu$ m, Brownlee, SPP, U.S.A.). The mobile phase consisted of 90% methanol and 10% DI water at a flow rate of 1.0 mL/min. The sorbed concentrations of PHE by sorbents were calculated by mass difference.

#### ■ RESULTS AND DISCUSSION

Characterization of Nano-BC and Goethite. Surface elemental composition and porosity of both nano- and bulk-BC are listed in Table S2. Nano400 and nano700 have much higher polarity index [(O+N)/C] and contents of Si and Ca than bulk400 and bulk700, suggesting that nano-BC contains more polar functional groups and crystalline inorganics and,

**Environmental Science & Technology** 

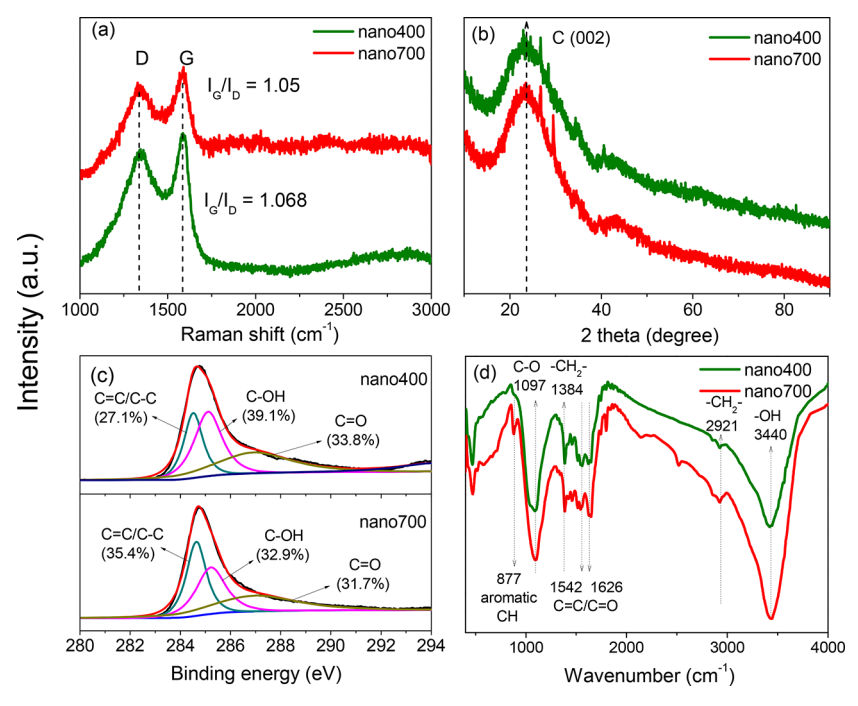


Figure 1. Characterization of nano-BC (nano400 and nano700). (a) Raman spectra; (b) XRD spectra; (c) high-resolution XPS C 1s spectra; and (d) FTIR spectra.

thus, higher surface activity. The polarity indexes are 0.633 and 0.606 for nano400 and nano700 in this study, similar to that of DBC derived from rice straw (0.59) and bamboo BC (0.55), respectively. For porous structure, the  $S_{\rm BET}$  and  $V_{\rm tot}$  of nano700 are significantly higher than nano400. Notably, the difference in  $S_{\rm BET}$  between nano700 and nano400 is much higher than that between bulk700 and bulk400, indicating that the release of volatile matter (e.g., CO, CO<sub>2</sub>, and  $C_xH_yO_z$ ) from carbon skeleton is probably easier for nanosized BC than bulky BC due to the lower steric hindrance effect. These results reveal that nano-BC has distinct physicochemical properties and would participate in more diverse biogeochemical processes in the environment relative to bulk BC.

The structural properties of nano400 and nano700 were examined using complementary spectroscopic techniques including Raman, X-ray diffraction (XRD), XPS, and FTIR (Figure 1). The Raman spectra exhibit two characteristic peaks at ~1350 cm<sup>-1</sup> (D band) and ~1580 cm<sup>-1</sup> (G band), which can be assigned to sp3 and sp2 carbon configuration, respectively. The intensity ratios of G to D bands  $(I_G/I_D)$ are very close to 1.0 for both nano400 (1.068) and nano700 (1.05), suggesting that they have comparable contents of amorphous and graphitic carbon. This is different from many previous observations for bulk biochar where the graphitization degree generally increases with increasing HTT. 34,35 For example, Xie et al.34 showed that the biochar prepared at 500 °C had higher ratio of  $I_G/I_D$  (2.2) than that of produced at 400 °C (2.0). Similarly, the  $I_G/I_D$  ratios of sewage sludge biochar were found to increase with increasing HTT, indicating a conversion of amorphous carbon to graphene domain.<sup>35</sup> Our Raman spectra results indicate that nano-BC has a higher content of amorphous C structure and relatively smaller crystallite size<sup>36</sup> compared with bulk BC. The broad XRD peaks of nano400 and nano700 centered at 22° (Figure 1b) also demonstrate the presence of highly disordered carbon atoms. The functional groups present on the surface of nano-

BC were examined by XPS. The C 1s spectra can be deconvoluted into three major peaks at 284.6 eV (C—C/C= C), 285.2 eV (C-OH), and 286.7 eV (C-O), respectively. <sup>37,38</sup> As shown in Figure 1c, the peak area percent of C— C/C=C in nano700 (35.4%) is higher than that in nano400 (27.1%), suggesting that nano700 has more content of sp<sup>2</sup>- and sp<sup>3</sup>-hybridized carbon configurations due to higher HTT. By contrast, nano400 has a higher content of O-containing groups including hydroxyl (39.1%) and carboxyl (33.8%) than nano700 (32.9% for -OH and 31.7% for -COOH), indicative of the higher polarity and surface charge density of nano400. Surface functional groups of nano-BC were also probed by FTIR (Figure 1d), including -OH at 3440 cm<sup>-1</sup>, -CH<sub>2</sub> at 2921 and 1384 cm<sup>-1</sup>, aromatic C=C and/or C=O stretching between 1626 and 1542 cm<sup>-1</sup>, C-O at 1097 cm<sup>-1</sup>, and aromatic C—H at 877 cm<sup>-1</sup>. The higher intensity of nano700 from vibration of aromatic C=C/C=O and C-H bands denotes its higher degree of condensation and aromaticity than nano400, consistent with the XPS data.

Colloidal Stability of Nano-BC and Goethite. The size distribution of nano-BC and goethite after 20 min sonication is presented in Figure S3, where the D<sub>h</sub> of nano400 (~280 nm) and nano700 (~220 nm) remained constant during the test time at an unadjusted pH (5.3); however, that of goethite gradually increased from 700 to 1200 nm at the same condition. After sonication for another 60 min, the  $D_h$  of goethite greatly decreased and remained at 400-600 nm (Figure S4). Thus, the nano-BC is more stable to homoaggregation than the goethite colloids. Therefore, all the goethite samples employed in the following heteroaggregation were sonicated for 80 min before use to keep them relatively stable. As shown in Figure S5a, the zeta potential of nano-BC decreased from around -5 to -40 mV when the solution pH increased from 2 to 10; meanwhile, that of goethite decreased from around 30 to -20 mV, and its isoelectric point was ~6. The negative zeta potential of nanoBC over the entire pH range is indicative of a stable suspension. Given the limitation of zeta potential to directly reflect the surface charge density of colloidal particles, <sup>39</sup> surface potentials ( $\Psi_{\rm o}$ ) of nano400 and nano700 were directly determined from measured EPM values via Henry equation, <sup>40</sup> and the values for nano400 and nano700 are -6.11 and -5.30 mV, respectively. The detailed calculation is presented in the Supporting Information.

Homoaggregation kinetics of nano-BC was examined in a range of NaCl or  $CaCl_2$  concentrations. The attachment efficiencies ( $\alpha$ ) of nano-BC as a function of electrolyte concentration at different pHs are given in Figure 2a. The

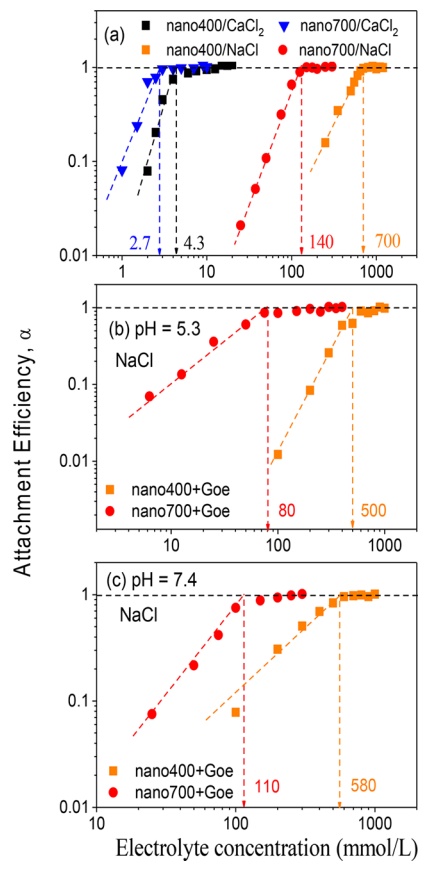


**Figure 2.** Attachment efficiencies of BC nanoparticles (nano400 and nano700) as a function of NaCl or CaCl<sub>2</sub> concentration at an unadjusted pH (5.3) (a) and the influence of goethite (Goe) on attachment efficiencies of BC nanoparticles at pH 5.3 (b) and 7.4 (c), respectively. The concentrations of nano-BC and goethite were 20 and 50 mg/L, respectively.

corresponding aggregation profiles are shown in Figures S6 and S7. Both reaction- and diffusion-limited aggregation regimes can be observed in the measurements, consistent with the classic DLVO theory. The attachment efficiencies ( $\alpha$ ) of nanoparticles increased with increasing electrolyte concentration until approaching 1 when the CCC was achieved. The CCC values of nano400 were up to 700 mmol/L for Na<sup>+</sup> and 4.3 mmol/L for Ca<sup>2+</sup>, and those of nano700 were 140 mmol/L for Na<sup>+</sup> and 2.7 mmol/L for Ca<sup>2+</sup>, respectively, at an unadjusted pH (5.3). The ratios of CCC for nano400 and nano700 in CaCl<sub>2</sub> to NaCl are  $2^{-7.35}$  and  $2^{-5.80}$ , respectively, which is basically consistent with the prediction of the Schulze–Hardy model ( $z^{-6}$ , where z represents the cation

valence).  $^{41,42}$  The higher CCC of nano400, especially in NaCl, is attributed to its higher surface charge density due to plenty of O-containing groups, although the  $D_{\rm h}$  of nano400 is larger than that of nano700 (Figure S3). The result suggests that the aggregation behavior of nano-BC is determined not only by particle size but also by surface charge, and the latter is highly dependent on HTT. Table S3 lists the CCC values of several carbonaceous nanomaterials with NaCl and CaCl $_2$ , where the CCC of nano400 in NaCl is much higher than the others, indicating its greater stability in aqueous solutions. We also examined the CCCs of nano400 and nano700 at a weak alkaline condition (pH 7.4) and found that the values did not change greatly (Figure S8), showing that the nano-BC could remain stable in a variety of natural freshwater and soil environments.

Heteroaggregation of Nano-BC with Goethite. The CCCs of nano400 and nano700 in NaCl were greatly decreased by the presence of goethite at pH 5.3 and 7.4 (Figure 2b and c), respectively; hence, goethite could interact with nano-BC and affect its stability. The heteroaggregation at pH 5.3 can be mainly explained by the electrostatic attraction between negatively charged nano-BC and positively charged goethite. At pH 7.4, however, both nano-BC and goethite were negatively charged according to their zeta potentials (Figure S5a). Thus, additional interaction(s) may contribute to the attachment of nano-BC to goethite at pH 7.4.

The heteroaggregation rates of nano-BC with goethite were only determined at pH 5.3 because the electrostatic repulsion greatly prevented the Dh growth of BC-goethite heteroaggregates at pH 7.4 (Figure S9). At pH 5.3, the D<sub>h</sub> of BCgoethite mixture significantly increased with increasing BCgoethite mass ratio due to the favorable heteroaggregation between the two oppositely charged particles (Figure 3a and b). For comparison, the homoaggregation rates of nano400 and nano700 under diffusion-limited conditions are plotted in Figure 3c. It is shown that the maximum heteroaggregation rates of goethite with nano400 (6.18 nm/min) and nano700 (8.12 nm/min) are significantly higher than the respective homoaggregation rates of nano400 (3.99 nm/min) and nano700 (6.62 nm/min). The maximum heteroaggregation rates were obtained as the concentration of nano400 and nano700 reached 0.4 and 0.64 mg TOC/L, respectively, which corresponded to the mass ratio of 0.008 for nano400-goethite and 0.0128 for nano700-goethite. The lower ratio of nano400 suggests that it may be more effective in dispersing goethite than nano700 due to its higher surface charge density. The zeta potential changes of BC-goethite heteroaggregates with increasing BC concentrations are shown in Figure S5b. The zeta potential decreased greatly with BC concentration and approached zero when the concentrations of nano400 and nano700 were up to 0.4 and 0.6 mg TOC/L, respectively, which is consistent with the concentration at which the maximum heteroaggregation rate occurred (Figure 3c). The lower zeta potential of nano400-goethite heteroaggregate indicates its higher stability than that of nano700-goethite cluster. Figure S5a also depicts the zeta potential variations of BC-goethite heteroaggregates as a function of pH. The zeta potential of formed heteroaggregates is much lower (up to -20mV) than that of the bare goethite, indicating the enhanced dispersibility of goethite by attached nano-BC.

**Enhanced Dispersion of Goethite by Nano-BC.** The dispersion of goethite in the suspension of nano-BC was also measured by sedimentation kinetics experiments. At pH 5.3,

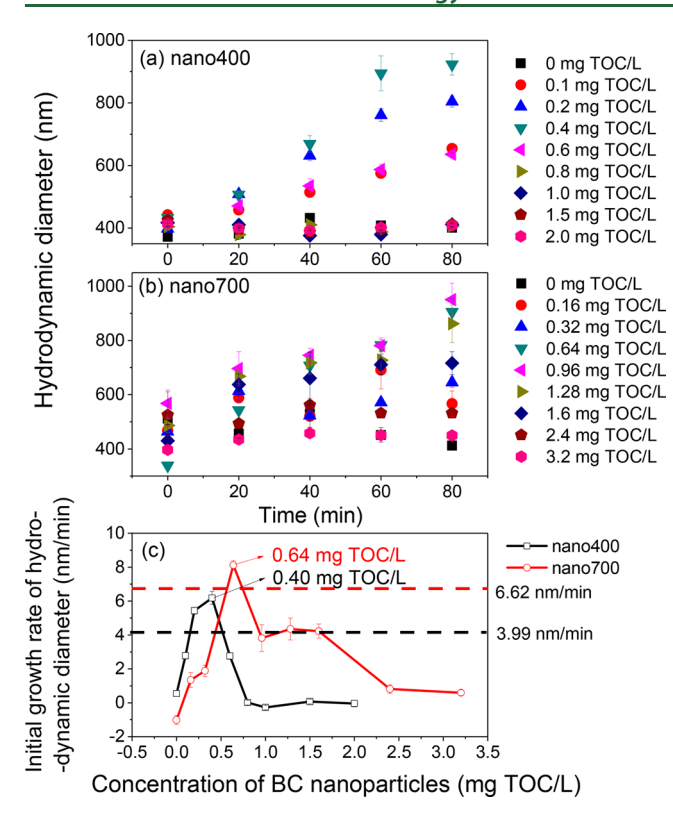


**Figure 3.** Heteroaggregation profiles of BC nanoparticles (nano400 and nano700) and goethite (Goe) with increasing concentration of nano-BC at pH 5.3. Error bars represent standard deviations of six samples (a, b). Initial growth rates of hydrodynamic diameter of the heteroaggregates as a function of nano-BC concentration at pH 5.3 (c). The concentration of goethite is 50 mg/L.

the bare goethite settled down completely within 4–8 h; meanwhile, very low concentrations of nano-BC had little effect on improving its dispersion (Figure 4). However, when the concentrations of nano400 and nano700 increased higher than 1.307 and 2.277 mg TOC/L, respectively, the sedimentation rate of goethite was greatly reduced during the period of 48 h. The enhanced dispersion of goethite by nano-BC can be seen more clearly from the photographs of the

corresponding goethite-BC mixtures after undisturbed standing for 48 h (Figure S10). The critical concentration ( $C_c$ ) of nano-BC to enhance goethite dispersion was ~1 mg TOC/L for nano400 and 2 mg TOC/L for nano700, respectively. When the concentration of nano-BC was higher than its  $C_{ct}$  the color of the mixtures changed into light brown and then to dark brown with increasing BC concentration demonstrating the enhanced dispersion of goethite. On the other hand, goethite also can be well-dispersed at pH 7.4, but the  $C_c$  of nano400 and nano700 increased to ~1.9 and 3.0 mg TOC/L (Figure S11), respectively, suggesting that nano-BC had lower adhesion affinity to goethite at this pH condition. To further support the observation, the pH effect on dispersion of nano-BC, goethite, and their aggregates was examined, respectively (Figures S12 and S13). Both nano400 and nano700 were deposited at pH 2 by forming aggregates due to decreased negative charge, but they can be well-dispersed in the pH range of 4-10, which is similar to other carbonaceous nanomaterials such as GO<sup>43</sup> and carbon nanotubes. <sup>18</sup> For goethite, however, most of the particles quickly settled in the pH of 2 to 6 until the pH increased to 8-10 where the goethite was welldispersed because of the abundance of negative charges at the highly basic condition. Note that the goethite can be welldispersed with the presence of nano-BC at a wide pH range (4-8), illustrating that other interactions also contribute to the adhesion of nano-BC to goethite besides electrostatic attraction. Previous studies showed that carbonaceous nanomaterials can interact with goethite through H-bonding and/or Lewis acid—base interactions. <sup>22</sup> The  $pK_a$  values of carboxyl and phenolic hydroxyl groups are around 4.3 and 9.8, respectively.<sup>21</sup> Thus, at the tested pH conditions (5.3 and 7.4), Hbonding can be formed between the hydroxyl groups on the surface of goethite and oxyl groups on the nano-BC (especially nano400). Lewis acid-base interactions could also contribute to their association, wherein the hydroxyl groups serve as Lewis base due to the lone electron pairs of oxygen atoms, and Lewis acid centers can be formed on BC surface because of electron-withdrawal capacity by its O-containing groups. Both hydrogen-bonding and Lewis acid-base interactions may overcome the electrostatic repulsion and lead to the relatively weak attachment of nano-BC on goethite at pH 7.4.

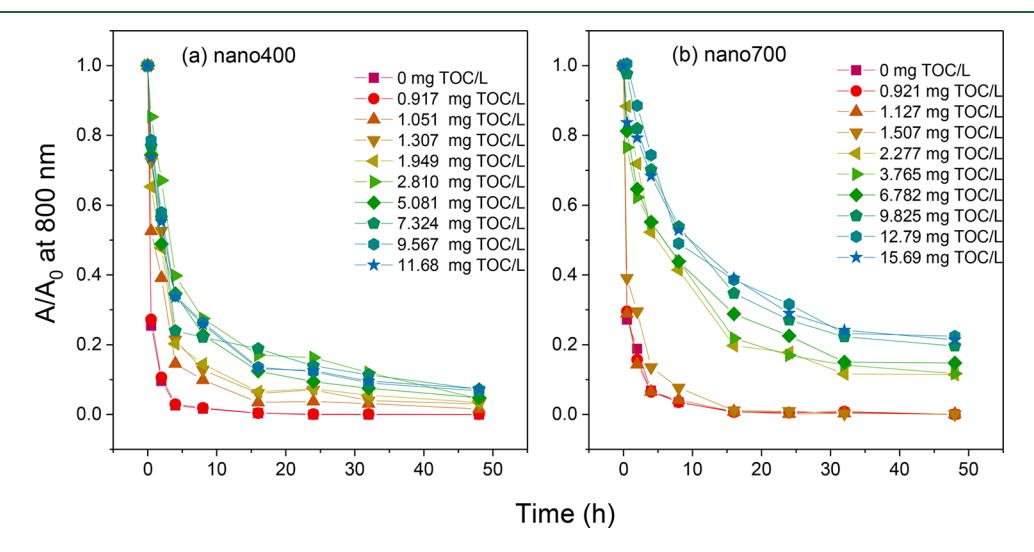


Figure 4. Sedimentation kinetics of BC nanoparticle (nano400 and nano700)-goethite heteroaggregates with increasing BC concentration. The concentration of goethite was 1000 mg/L.

Consistently, the results show that the attachment capacities of goethite for nano400 and nano700 are around 2 and 1 mg TOC/g, respectively, in the tested BC concentrations (Figure S14). The attachment capacity of goethite for nano700 is almost the same to that of other iron oxide minerals (e.g., hematite) for GO,<sup>23</sup> indicating similar surface properties of nano-700 and GO. The higher attachment of nano400 can be attributed to the stronger electrostatic attraction and/or its higher content of O-containing groups. Surface-potential-normalized attachments of nano-BC on goethite were compared to directly illustrate the effect of functional groups on the interaction (Figure S15), where the large difference in the normalized attachment demonstrated the crucial role of oxyl groups in the enhanced attachment of nano400.

Given the larger particle size of nano400 (Figure S1), it is likely that the attached nano400 has a higher surface coverage per particle on goethite than nano700. We calculated the BC-goethite mass ratios at  $C_{\rm c}$  of nano400 and nano700, respectively, where the mass ratio (0.001) of nano400 is lower than that (0.002) when the attachment equilibrium of nano400 on goethite is achieved, but the mass ratio (0.002) of nano700 is higher than that (0.001) when the attachment equilibrium of nano700 is obtained. The results suggest that goethite could be well-dispersed by nano400 before its complete attachment is reached, while additional nano700 particles are needed to effectively disperse goethite after the attachment, indicating that the dispersion of mineral colloids is mainly dependent on the surface charge of nano-BC and the attachment capacity on minerals.

Sorption of PHE by BC-Goethite Heteroaggregates. As expected, nano-BC has a much higher sorption affinity for PHE than goethite verified by the higher distribution coefficients  $(K_d)$  (Figure S16). Thus, it is likely that the sorption of HOCs on minerals would have been enhanced via heteroaggregation with nano-BC in aqueous solutions.4 However, we found for the first time that both BC-goethite mass ratio and solute concentration play a critical role in manipulating the PHE sorption on BC-goethite heteroaggregates. As depicted in the gray area of Figure 5, for a lower concentration of PHE (i.e., 0.236 and 0.526 mg/L), the sorption of PHE showed little increase at low BC concentrations and then significantly increased when it was higher than ~0.4 and 0.6 mg TOC/L for nano400 and nano700, respectively. Interestingly, these concentrations were consistent with those at which the maximum heteroaggregation rates of goethite and nano-BC occurred as mentioned above (i.e., 0.4 mg TOC/L for nano400 and 0.64 mg TOC/L for nano700) (Figure 3), which directly demonstrates that BCgoethite mass ratio could control the configuration of heteroaggregates and consequently affect the sorption patterns for organic chemicals.

For a higher concentration of PHE (i.e., 0.79 mg/L), however, its sorption significantly increased with the introduction of nano-BC, and no plateau for PHE sorption was observed at low nano-BC concentrations (the gray area in Figure 5), indicating its different sorption pattern. Recently, morphology transformation of a biomass-converted nanomaterial induced by the sorption of naphthalene (NAPH) and PHE was reported. The authors suggested that the formation of ordered structure was ascribed to the sorbate molecule-induced self-assembly of graphene nanosheets. Additionally, Yang et al. found that negative charges on the surface of BC colloids can be significantly shielded by the sorbed NAPH,

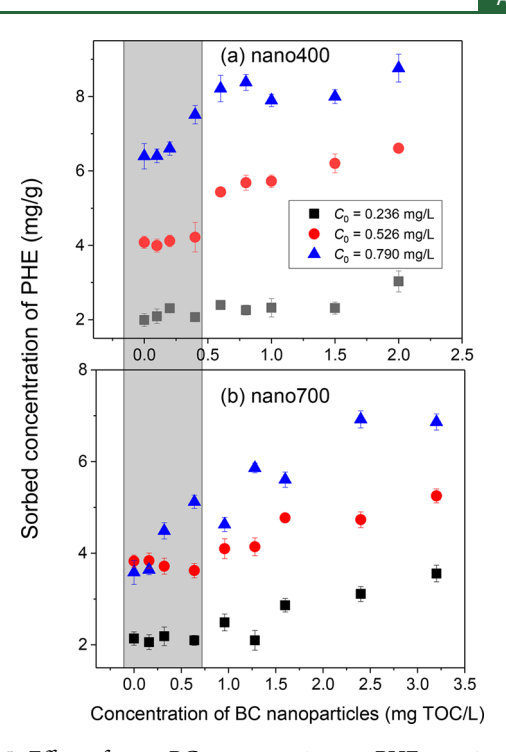


**Figure 5.** Effect of nano-BC concentration on PHE sorption by the BC-goethite heteroaggregates (n=3). The gray area denotes the different sorption patterns of PHE on the heteroaggregates at different concentrations of PHE; i.e., the sorption of PHE almost did not increase with increasing BC concentrations at low PHE concentrations, while it increased significantly at higher PHE concentration. The concentration of goethite was 50 mg/L.

which reduced the mobility of BC colloids in porous media. These results reveal that the structure of BC-goethite heteroaggregates may be relatively incompact and the surface charge of nano-BC could be modified by PHE sorption; therefore, the PHE molecules with a sufficiently high concentration are likely to (1) enter into the interior of BC-goethite heteroaggregates or (2) alter the configuration of heteroaggregates due to strong sorption affinity to BC, which may result in different sorption patterns compared with that at low concentrations of PHE.

Mechanism of Heteroaggregation between Nano-BC and Goethite. The representative TEM images of nano-BC and goethite are presented in parts a and b of Figure 6, respectively, and more images of nano400 and nano700 can be found in Figure S17. Parts c and d of Figure 6 exhibit the configurations of nano700-goethite heteroaggregates at two different mass ratios (i.e., 0.008 and 0.04). These mass ratios were selected based on the observation that the maximum heteroaggregation rate was obtained as the nano700-goethite mass ratio was 0.008 at an unadjusted pH condition (5.3). It is evident that plenty of nano700 and goethite can bind together to form bigger clusters when the mass ratio is 0.008, where the nano700 played an important bridging role in connecting different goethite particles (Figure 6c). However, when the BC-goethite mass ratio increased to 0.04, the majority of goethite surface was covered by nano700 and the bridging effect was greatly inhibited. As a result, the bigger clusters split into smaller BC-goethite heteroaggregates (Figure 6d). On the other hand, at a weak alkaline condition (pH = 7.4) where both nano-BC and goethite were negatively charged, they can only bind to form small clusters due to the hindrance of **Environmental Science & Technology** 

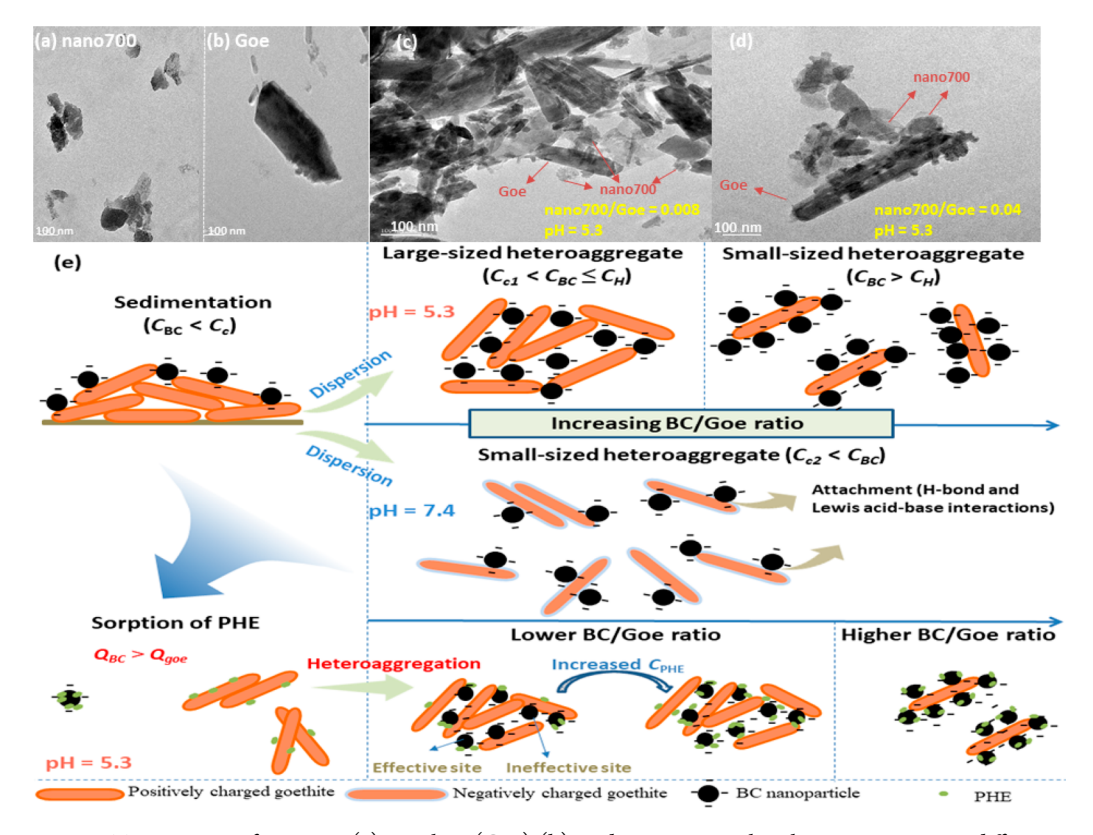


Figure 6. Representative TEM images of nano700 (a), goethite (Goe) (b), and nano700-goethite heteroaggregates at different mass ratios at pH 5.3 (c and d) as well as the proposed mechanism of BC-Goe heteroaggregation and its effect on the sorption of phenanthrene (PHE) (e).  $C_{\rm BC}$  and  $C_{\rm PHE}$  denote the concentration of nano-BC and PHE in the aqueous solution, respectively; both  $C_{\rm c1}$  and  $C_{\rm c2}$  denote the critical concentration of nano-BC to enhance the dispersion of goethite at pH 5.3 and 7.4, respectively;  $C_{\rm H}$  denotes the nano-BC concentration at which the maximum heteroaggregation rates occurred at pH 5.3; and  $Q_{\rm BC}$  and  $Q_{\rm goe}$  denote the sorption capacity of nano-BC and goethite for PHE, respectively.

electrostatic repulsion (Figure S18). Meanwhile, we noticed that the  $D_{\rm h}$  of heteroaggregates was independent of the BC-goethite mass ratio (0.008–0.04) at pH 7.4. These observations are consistent with our DLS results shown in Figures 3 and S9.

On the basis of the above TEM results, the possible mechanisms for BC-goethite heteroaggregation at different mass ratios and the corresponding impact on goethite sorption for PHE are proposed and illustrated in Figure 6e. At very low BC concentration, nano-BC has little effect on increasing the dispersion of goethite because the enhanced dispersibility by attached nano-BC is not sufficient enough to overcome its deposition potential. When the concentration of BC is higher than its  $C_c$  (i.e.,  $C_{BC} > C_c$ ), the goethite can be effectively dispersed via heteroaggregation with nano-BC. After that, there are two different situations: (1) At pH 5.3, the positively charged goethite can strongly bind with the negatively charged BC through electrostatic attraction to form primary heteroaggregates, and then the attached BC, serving as a bridge, can also interact with other goethite colloids to form large-sized heteroaggregates when the  $C_{BC}$  is in a range of  $C_c$  to  $C_H$  (i.e.,  $C_{\rm c}$  <  $C_{\rm BC}$   $\leq C_{\rm H}$ ).  $C_{\rm H}$  is the concentration at which the maximum heteroaggregation rate occurs. As  $C_{\rm BC}$  further increased (i.e.,  $C_{BC} > C_{H}$ ), nano-BC binds to the surface of goethite to form a negatively charged shell around it, 17 which greatly inhibits the occurrence of BC-bridge because most of the active sites on goethite are occupied by nano-BC. In that case, the BC-goethite clusters could only maintain their primary structure (i.e., small-sized heteroaggregates), which is more stable than the larger aggregates. (2) At pH 7.4, although

both goethite and nano-BC are negatively charged, they can also bind with each other to some extent via H-bonding and Lewis acid—base interactions as indicated by the attachment result and TEM observation (Figures S11 and S18). Due to the negatively charged nature of both nano-BC and goethite at this weak alkaline condition, the large-sized heteroaggregates could not be formed via the BC-bridge mechanism and only small-sized heteroaggregates can be observed.

Figure 6e also illustrates the sorption mechanism of PHE on BC-goethite heteroaggregates with different mass ratios at an unadjusted pH condition. Nano-BC has much higher sorption affinity for PHE than goethite as shown in Figure S16 (i.e.,  $Q_{\rm BC}$  $> Q_{\rm goe}$ ). However, the attached BC could not greatly increase the sorption of goethite at low BC-goethite ratios (i.e.,  $C_c$  <  $C_{\rm BC} \leq C_{\rm H}$ ) due to the formation of large-sized heteroaggregates, where a number of BC particles are probably wrapped into the interior of the heteroaggregates and become ineffective sorption sites. However, with increasing PHE concentration, the PHE molecules could penetrate into and alter the configuration of heteroaggregates, making the wrapped nano-BC become effective for PHE sorption (Figure 5). At high BC-goethite ratios (i.e.,  $C_{\rm BC} > C_{\rm H}$ ), only small-sized heteroaggregates are formed, and thus most of the attached BC particles are located on the surface of goethite and can effectively enhance the goethite sorption for PHE.

**Environmental Implication.** Nano-BC has unique physicochemical properties and can be released from bulk BC materials, participating in various environmental processes. The aggregation results indicate that nano-BC with higher surface potential and oxyl groups is expected to be more stable

to homoaggregation, wherein HTT is one of the dominating factors in regulating its colloidal behavior in aqueous environments. Nano-BC could enhance dispersibility of mineral colloids through heteroaggregation when the concentration of nano-BC exceeds its  $C_c$ , which mainly depends on the surface potential of nano-BC and its attachment affinity to minerals. Given the relatively low  $C_c$  of nano-BC to disperse minerals (e.g., goethite), it is foreseeable that the mineral colloids are likely to be dispersed when encountering nano-BC in natural aqueous systems despite the generally low mass ratio of nano-BC to minerals. Conversely, at higher concentrations of nano-BC, mineral colloids could lead to the deposition of nano-BC by attaching and forming large particulates, which have a weak colloidal stability. Thus, the effect of BC-mineral interactions on carbon storage and flux in the terrestrial ecosystem needs further study. Moreover, we found that the sorption of PHE was regulated by the configuration of BCgoethite heteroaggregates. A number of active sorption sites (mainly nano-BC) might be wrapped into the interior of the large-sized BC-mineral clusters and contribute little to the sorption of PHE. By contrast, the small-sized clusters exhibit higher sorption capacity for PHE. Thus, it should be noted that nano-BC can not only contribute to the dispersion of minerals but also make them efficient sorbents and potential carriers for organic compounds by forming stable clusters in the environments. Therefore, besides nano-BC itself, the BCmineral heteroaggregates should also be considered when evaluating the transport and related environment risk of nano-BC. In addition, how and to what extent the sorbate molecule could induce the structural transformation of BC-mineral heteroaggregates deserve more detailed investigations in the future.

### ASSOCIATED CONTENT

# S Supporting Information

The Supporting Information is available free of charge on the ACS Publications website at DOI: 10.1021/acs.est.8b05066.

Determination of  $\alpha$ , CCCs, and surface potentials of nano-BC;  $D_{\rm h}$  of goethite and nano-BC; attachment kinetics; zeta potentials; aggregation of nano-BC; heteroaggregation of nano-BC and goethite at pH 7.4; photographs of BC-goethite mixtures; UV-vis of goethite; sorption of PHE; TEM images; and selected physicochemical properties of nano- and bulk-BC (PDF)

#### AUTHOR INFORMATION

# **Corresponding Author**

\*Phone: 413-545-5212; e-mail: bx@umass.edu.

ORCID ®

Fei Lian: 0000-0002-9372-511X Zhenyu Wang: 0000-0002-5114-435X Baoshan Xing: 0000-0003-2028-1295

# Notes

The authors declare no competing financial interest.

# ACKNOWLEDGMENTS

We gratefully acknowledge financial support from the National Natural Science Foundation of China (41573127), China Scholarship Council (201503250054), for F.L. to study at

UMass Amherst, USDA McIntire-Stennis Program (MAS 00028), and NSF (CBET 1739884).

#### REFERENCES

- (1) Song, Y.; Wang, F.; Kengara, F. O.; Yang, X.; Gu, C.; Jiang, X. Immobilization of chlorobenzenes in soil using wheat straw biochar. *J. Agric. Food Chem.* **2013**, *61* (18), 4210–4217.
- (2) Singh, B. P.; Cowie, A. L.; Smernik, R. J. Biochar carbon stability in a clayey soil as a function of feedstock and pyrolysis temperature. *Environ. Sci. Technol.* **2012**, *46* (21), 11770–11778.
- (3) Silber, A.; Levkovitch, I.; Graber, E. R. pH-dependent mineral release and surface properties of cornstraw biochar: agronomic implications. *Environ. Sci. Technol.* **2010**, *44* (24), 9318–9323.
- (4) Jha, P.; Biswas, A. K.; Lakaria, B. L.; Rao, A. S. Biochar in agriculture prospects and related implications. *Curr. Sci. India* **2010**, 99 (9), 1218–1225.
- (5) Dittmar, T.; Paeng, J.; Gihring, T. M.; Suryaputra, I. G. N. A.; Huettel, M. Discharge of dissolved black carbon from a fire-affected intertidal system. *Limnol. Oceanogr.* **2012**, *57* (4), 1171–1181.
- (6) Roebuck, J. A., Jr.; Seidel, M.; Dittmar, T.; Jaffe, R. Land use controls on the spatial variability of dissolved black carbon in a subtropical watershed. *Environ. Sci. Technol.* **2018**, 52 (15), 8104–8114
- (7) Xu, C.; Xue, Y.; Qi, Y.; Wang, X. Quantities and fluxes of dissolved and particulate black carbon in the changjiang and huanghe rivers, China. *Estuaries Coasts* **2016**, *39* (6), 1617–1625.
- (8) Dittmar, T.; Paeng, J. A heat-induced molecular signature in marine dissolved organic matter. *Nat. Geosci.* **2009**, 2 (3), 175–179.
- (9) Jaffe, R.; Ding, Y.; Niggemann, J.; Vahatalo, A. V.; Stubbins, A.; Spencer, R. G. M.; Campbell, J.; Dittmar, T. Global charcoal mobilization from soils via dissolution and riverine transport to the oceans. *Science* **2013**, *340* (6130), 345–347.
- (10) Spokas, K. A.; Novak, J. M.; Masiello, C. A.; Johnson, M. G.; Colosky, E. C.; Ippolito, J. A.; Trigo, C. Physical disintegration of biochar: An overlooked process. *Environ. Sci. Technol. Lett.* **2014**, *1* (8), 326–332.
- (11) Qian, L. B.; Zhang, W. Y.; Yan, J. C.; Han, L.; Gao, W. G.; Liu, R. Q.; Chen, M. F. Effective removal of heavy metal by biochar colloids under different pyrolysis temperatures. *Bioresour. Technol.* **2016**, 206, 217–224.
- (12) Grolimund, D.; Borkovec, M.; Barmettler, K.; Sticher, H. Colloid-facilitated transport of strongly sorbing contaminants in natural porous media: A laboratory column study. *Environ. Sci. Technol.* **1996**, *30* (10), 3118–3123.
- (13) Wigginton, N. S.; Haus, K. L.; Hochella, M. F., Jr. Aquatic environmental nanoparticles. *J. Environ. Monit.* **2007**, 9 (12), 1306–1316.
- (14) Philippe, A.; Schaumann, G. E. Interactions of dissolved organic matter with natural and engineered inorganic colloids: A review. *Environ. Sci. Technol.* **2014**, 48 (16), 8946–8962.
- (15) Xu, F.; Wei, C.; Zeng, Q.; Li, X.; Alvarez, P. J. J.; Li, Q.; Qu, X.; Zhu, D. Aggregation behavior of dissolved black carbon: Implications for vertical mass flux and fractionation in aquatic systems. *Environ. Sci. Technol.* **2017**, *51* (23), 13723–13732.
- (16) Chen, C.; Huang, W. Aggregation kinetics of diesel soot nanoparticles in wet environments. *Environ. Sci. Technol.* **2017**, *51* (4), 2077–2086.
- (17) Yi, P.; Pignatello, J. J.; Uchimiya, M.; White, J. C. Heteroaggregation of cerium oxide nanoparticles and nanoparticles of pyrolyzed biomass. *Environ. Sci. Technol.* **2015**, 49 (22), 13294–13303.
- (18) Saleh, N. B.; Pfefferle, L. D.; Elimelech, M. Aggregation kinetics of multiwalled carbon nanotubes in aquatic systems: Measurements and environmental implications. *Environ. Sci. Technol.* **2008**, 42 (21), 7963–7969.
- (19) Mashayekhi, H.; Ghosh, S.; Du, P.; Xing, B. Effect of natural organic matter on aggregation behavior of C60 fullerene in water. *J. Colloid Interface Sci.* **2012**, *374* (1), 111–117.

- (20) Wu, L.; Liu, L.; Gao, B.; Muñoz-Carpena, R.; Zhang, M.; Chen, H.; Zhou, Z.; Wang, H. Aggregation kinetics of graphene oxides in aqueous solutions: Experiments, mechanisms, and modeling. *Langmuir* **2013**, 29 (49), 15174–15181.
- (21) Zhao, J.; Liu, F.; Wang, Z.; Cao, X.; Xing, B. Heteroaggregation of graphene oxide with minerals in aqueous phase. *Environ. Sci. Technol.* **2015**, 49 (5), 2849–2857.
- (22) Liu, X.; Li, J.; Huang, Y.; Wang, X.; Zhang, X.; Wang, X. Adsorption, aggregation, and deposition behaviors of carbon dots on minerals. *Environ. Sci. Technol.* **2017**, *51* (11), 6156–6164.
- (23) Feng, Y.; Liu, X.; Huynh, K. A.; McCaffery, J. M.; Mao, L.; Gao, S.; Chen, K. L. Heteroaggregation of graphene oxide with nanometerand micrometer-sized hematite colloids: Influence on nanohybrid aggregation and microparticle sedimentation. *Environ. Sci. Technol.* 2017, 51 (12), 6821–6828.
- (24) Huynh, K. A.; McCaffery, J. M.; Chen, K. L. Heteroaggregation of multiwalled carbon nanotubes and hematite nanoparticles: Rates and mechanisms. *Environ. Sci. Technol.* **2012**, *46* (11), 5912–5920.
- (25) Jin, J.; Sun, K.; Wang, Z.; Yang, Y.; Han, L.; Xing, B. Characterization and phenanthrene sorption of natural and pyrogenic organic matter fractions. *Environ. Sci. Technol.* **2017**, *51* (5), 2635–2642.
- (26) Qu, X.; Fu, H.; Mao, J.; Ran, Y.; Zhang, D.; Zhu, D. Chemical and structural properties of dissolved black carbon released from biochars. *Carbon* **2016**, *96*, 759–767.
- (27) Yu, X. Y.; Ying, G. G.; Kookana, R. S. Sorption and desorption behaviors of diuron in soils amended with charcoal. *J. Agric. Food Chem.* **2006**, *54* (22), 8545–8550.
- (28) Jeong, S.; Wander, M. M.; Kleineidam, S.; Grathwohl, P.; Ligouis, B.; Werth, C. J. The role of condensed carbonaceous materials on the sorption of hydrophobic organic contaminants in subsurface sediments. *Environ. Sci. Technol.* **2008**, 42 (5), 1458–1464.
- (29) Tang, J. X.; Weber, W. J. Development of engineered natural organic sorbents for environmental applications. 2. Sorption characteristics and capacities with respect to phenanthrene. *Environ. Sci. Technol.* **2006**, 40 (5), 1657–1663.
- (30) Ghosh, S.; Pradhan, N. R.; Mashayekhi, H.; Dickert, S.; Thantirige, R.; Tuominen, M. T.; Tao, S.; Xing, B. Binary short-range colloidal assembly of magnetic iron oxides nanoparticles and fullerene (nC60) in environmental media. *Environ. Sci. Technol.* **2014**, 48 (20), 12285–12291.
- (31) Smith, B. M.; Pike, D. J.; Kelly, M. O.; Nason, J. A. Quantification of heteroaggregation between citrate-stabilized gold nanoparticles and hematite colloids. *Environ. Sci. Technol.* **2015**, 49 (21), 12789–12797.
- (32) Tang, Z.; Wu, L.; Luo, Y.; Christie, P. Size fractionation and characterization of nanocolloidal particles in soils. *Environ. Geochem. Health* **2009**, 31 (1), 1–10.
- (33) Huang, G.; Guo, H.; Zhao, J.; Liu, Y.; Xing, B. Effect of co-existing kaolinite and goethite on the aggregation of graphene oxide in the aquatic environment. *Water Res.* **2016**, *102*, 313–320.
- (34) Xie, M.; Chen, W.; Xu, Z.; Zheng, S.; Zhu, D. Adsorption of sulfonamides to demineralized pine wood biochars prepared under different thermochemical conditions. *Environ. Pollut.* **2014**, *186*, 187–194
- (35) Zhang, J.; Lu, F.; Zhang, H.; Shao, L.; Chen, D.; He, P. Multiscale visualization of the structural and characteristic changes of sewage sludge biochar oriented towards potential agronomic and environmental implication. *Sci. Rep.* **2015**, *5*, 9406.
- (36) Cancado, L. G.; Takai, K.; Enoki, T.; Endo, M.; Kim, Y. A.; Mizusaki, H.; Jorio, A.; Coelho, L. N.; Magalhaes-Paniago, R.; Pimenta, M. A. General equation for the determination of the crystallite size L-a of nanographite by Raman spectroscopy. *Appl. Phys. Lett.* **2006**, *88* (16), 163106.
- (37) Yang, Y.; Shu, L.; Wang, X.; Xing, B.; Tao, S. Impact of deashing humic acid and humin on organic matter structural properties and sorption mechanisms of phenanthrene. *Environ. Sci. Technol.* **2011**, 45 (9), 3996–4002.

- (38) Dong, X.; Ma, L. Q.; Zhu, Y.; Li, Y.; Gu, B. Mechanistic investigation of mercury sorption by brazilian pepper biochars of different pyrolytic temperatures based on X-ray photoelectron spectroscopy and flow calorimetry. *Environ. Sci. Technol.* **2013**, 47 (21), 12156–12164.
- (39) Smith, B.; Wepasnick, K.; Schrote, K. E.; Bertele, A. R.; Ball, W. P.; O'Melia, C.; Fairbrother, D. H. Colloidal properties of aqueous suspensions of acid-treated, multi-walled carbon nanotubes. *Environ. Sci. Technol.* **2009**, 43 (3), 819–825.
- (40) Li, K.; Zhao, X.; Hammer, B. K.; Du, S.; Chen, Y. Nanoparticles inhibit DNA replication by binding to dna: Modeling and experimental validation. *ACS Nano* **2013**, *7* (11), 9664–9674.
- (41) Overbeek, J. T. G. The rule of schulze and hardy. *Pure Appl. Chem.* **1980**, 52 (5), 1151–1161.
- (42) Elimelech, M.; Gregory, J.; Jia, X.; Williams, R. A. Particle deposition and aggregation: measurement, modelling and stimulation; Butterworth-Heinemann: Oxford, U.K., 1995.
- (43) Chowdhury, I.; Duch, M. C.; Mansukhani, N. D.; Hersam, M. C.; Bouchard, D. Colloidal properties and stability of graphene oxide nanomaterials in the aquatic environment. *Environ. Sci. Technol.* **2013**, 47 (12), 6288–6296.
- (44) Lian, F.; Xing, B. Black carbon (biochar) in water/soil environments: Molecular structure, sorption, stability, and potential risk. *Environ. Sci. Technol.* **2017**, *51* (23), 13517–13532.
- (45) Xiao, X.; Chen, B.; Zhu, L.; Schnoor, J. L. Sugar cane-converted graphene-like material for the superhigh adsorption of organic pollutants from water via coassembly mechanisms. *Environ. Sci. Technol.* **2017**, *51* (21), 12644–12652.
- (46) Yang, W.; Wang, Y.; Sharma, P.; Li, B.; Liu, K.; Liu, J.; Flury, M.; Shang, J. Effect of naphthalene on transport and retention of biochar colloids through saturated porous media. *Colloids Surf., A* **2017**, 530, 146–154.